ELSEVIER

International Journal of Mass Spectrometry 221 (2002) 209–218

International Journal of Mass Spectrometry

www.elsevier.com/locate/ijms

Study of ion/molecule reactions of atmospherically important negative ions with methane sulfonic acid

N. Schoon[a,*], C. Amelynck[a], P. Bultinck[b], E. Arijs[a]

[a] *Belgian Institute for Space Aeronomy, Ringlaan 3, B-1180 Brussels, Belgium*
[b] *Department of Inorganic and Physical Chemistry, Ghent University, Krijgslaan 281, S3, B-9000 Ghent, Belgium*

Received 14 June 2002; accepted 19 September 2002

Abstract

The ion/molecule reactions of O^-, O_2^-, $O_2^-{\cdot}H_2O$, O_3^-, NO_3^-, $NO_3^-{\cdot}HNO_3$, CO_3^-, CO_4^- and NO_2^- with methane sulfonic acid (MSA) have been studied at 300 K and 1.07 mb using the flowing afterglow technique. Most of the reactions give multiple products and the corresponding product yields have been deduced from the measurements. All the ion/molecule reactions, except for the $NO_3^-{\cdot}HNO_3$/MSA reaction, produce the $CH_3SO_3^-$ anion by proton transfer. The $NO_3^-{\cdot}HNO_3$/MSA reaction results in the formation of $CH_3SO_3^-{\cdot}HNO_3$ product ions. An additional association channel has been observed for the CO_3^- and the NO_2^-/MSA reaction. $O_2^-{\cdot}CH_3SO_3H$ has been identified as second reaction product of the CO_4^-/MSA reaction. $CH_2SO_3^-$ product ions are also formed by the reaction of O^- and CO_3^- with MSA. All ion/molecule reactions proceed within the experimental error at the collision rate. Several secondary product ions have also been observed and the corresponding reactions identified. The ground state geometry of MSA has been determined by quantum chemical calculations and a value of 3.776 D was found for the dipole moment and 6.71 $Å^3$ for the polarizability. (Int J Mass Spectrom 221 (2002) 209–218)

Keywords: Methane sulfonic acid; Ion/molecule reactions; Tropospheric trace gases; Chemical ionization

1. Introduction

According to Spiro et al. [1] approximately 12% of the global emissions of sulfur gases into the atmosphere is due to the marine biosphere. The major sulfur component emitted by the oceans is dimethyl sulfide (DMS), excreted by phytoplankton [2,3].

Laboratory studies [4,5] have shown that once DMS is released to the atmosphere, it is reacting with OH and NO_3 to form several oxidation products, which are eventually converted to sulfuric acid (H_2SO_4) and methane sulfonic acid (CH_3SO_3H, MSA). These low vapor pressure acids are believed to play an important role in the formation and growth mechanisms of tropospheric aerosols [6–8].

About 15 years ago Charlson et al. [9] have put forward the so-called CLAW hypothesis. They proposed a feedback mechanism involving the emission of DMS by marine phytoplankton due to effects of temperature and sunlight, the subsequent enhanced production of cloud condensation nuclei and cloud formation to counteract a possible warming and thus regulating the climate.

With respect to this theory, measurements of aerosols, cloud condensation nuclei and the homogeneous nucleation precursor gases, such as sulfuric acid and MSA, in the troposphere are extremely important.

* Corresponding author. E-mail: niels.schoon@bira-iasb.oma.be

1387-3806/02/$ – see front matter
PII S1387-3806(02)00998-3

Detection and quantification of both these acids in the gas phase in the troposphere have only been possible recently by chemical ionization mass spectrometry [10–12]. These measurements are based upon the ion/molecule reactions of sulfuric acid and MSA with $NO_3^-{\cdot}HNO_3$ ions. Tropospheric air is sampled into an effectively wall-less flow tube where H_2SO_4 and MSA are allowed to react with the $NO_3^-{\cdot}HNO_3$ source ions resulting in the formation of HSO_4^- and $CH_3SO_3^-$ core product ions, respectively. From the measurement of the rate of product to source ions with a mass spectrometer, the residence time of the ions in the flow tube and the rate constant of the ion/molecule reactions involved, the concentration of sulfuric acid and MSA can be derived.

Whereas for H_2SO_4 the rate constant of the reaction with $NO_3^-{\cdot}HNO_3$ has been measured [13], it is assumed that the $NO_3^-{\cdot}HNO_3$/MSA reaction occurs at approximately the same rate (collision frequency). Knowledge of the rate constant of the $NO_3^-{\cdot}HNO_3$/MSA reaction would reduce the uncertainty of the measurements.

MSA also plays an important role in the tropospheric ion chemistry. Recently a model of the tropospheric ion chemistry [14] has been set up which includes the ion/molecule reactions of MSA with several atmospheric ions. Again due to the lack of measurements it was assumed that the reactions took place at the collision rate.

To provide for the reaction rate constants required for the analysis of chemical ionization measurements and for modeling, we studied the reactions of MSA with possible atmospheric precursor ions, such as O^-, O_2^-, $O_2^-{\cdot}H_2O$, O_3^-, NO_3^-, $NO_3^-{\cdot}HNO_3$, CO_3^-, CO_4^- and NO_2^- using the flowing afterglow technique.

In addition, quantum chemical calculations have been performed to elucidate the structure of MSA and to determine values for the dipole moment and the polarizability of this molecule. This allowed us to calculate ion/molecule collision rate constants using the Su and Chesnavich approach [15] and to compare our experimental data with theory.

2. Experiment

The ion/molecule reactions, reported here, were studied at 300 K in a stainless steel flowing afterglow apparatus, which is shown schematically in Fig. 1. A detailed description of the experimental set-up being given in previous publications [16,17], only the major outlines will be presented here.

The instrument consists of a 40 mm inner-diameter flow tube coupled to a quadrupole mass spectrometer. The ions are convectively transported towards the detection chamber by a buffer gas flow, maintained by a roots pump, and are sampled through a 0.3 mm orifice in the mass spectrometer, where they are filtered according to their mass to charge ratio and detected by a channeltron operating in the pulse mode. The measurements were carried out at a flow tube pressure p_{FT} of 1.07 mb, corresponding to a 50–65 STP $cm^3\,s^{-1}$ flow of the N_2 buffer gas (99.999% purity), depending upon the gas flow through the ion source.

The ions are produced by means of a dc high voltage discharge, located at 118 cm upstream the mass spectrometer inlet.

By flowing a mixture of N_2 (typically 1.7 STP $cm^3\,s^{-1}$), CO_2 (∼0.04 STP $cm^3\,s^{-1}$) and O_2 (∼2.1 STP $cm^3\,s^{-1}$) through the discharge, NO_3^- ions are produced in the discharge according to the ion/molecule reactions described by Möhler and Arnold [18]. As some nitric acid impurities remained in the discharge tube from previous experiments, $NO_3^-{\cdot}HNO_3$ ions were also produced. Changing slightly the operating conditions of the discharge, allowed us to modify the relative intensity of the NO_3^- and $NO_3^-{\cdot}HNO_3$ ion signals.

CO_3^- and CO_4^- ions were formed by adding CO_2 (0.04–0.1 STP $cm^3\,s^{-1}$) and O_2 (2.5–3.3 STP $cm^3\,s^{-1}$) to an Ar flow (2.5–4.2 STP $cm^3\,s^{-1}$) through the discharge or by introducing the CO_2/O_2 mixture in the afterglow of the Ar discharge.

Similarly O_2^- and O_3^- ions were generated by establishing a discharge in a mixture of Ar and O_2 (4.2–10.8 STP $cm^3\,s^{-1}$ Ar, 1–3.3 STP $cm^3\,s^{-1}$ O_2) or by adding the O_2 flow to the Ar discharge afterglow. Again, the relative intensity of the CO_3^-/CO_4^- and

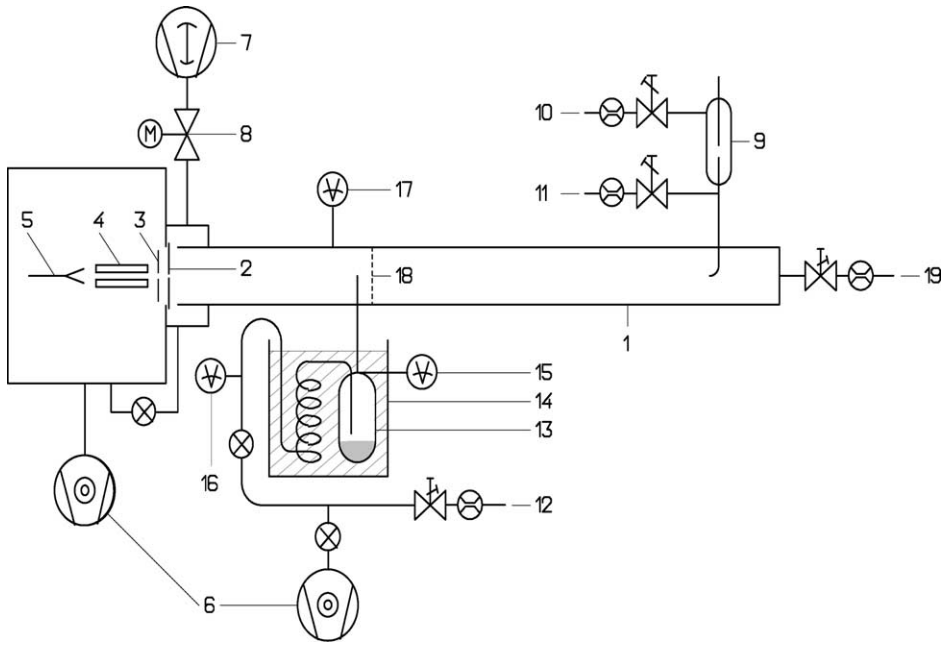

Fig. 1. Schematic representation of the laboratory apparatus. (1) Flow tube; (2) ion inlet plate; (3) electrostatic lens; (4) quadrupole mass filter; (5) channeltron electron multiplier; (6) turbomolecular pumps; (7) roots pump; (8) electronically controlled butterfly valve; (9) dc high voltage discharge ion source; (10) ion parent gas and Ar inlet (see text); (11) ion parent gas inlet (see text); (12) N_2 inlet; (13) MSA reservoir; (14) heated water bath; (15), (16) and (17) pressure sensors; (18) grid; (19) buffer gas inlet. During the measurements with MSA pressure sensor (15) was removed to prevent condensation of MSA. Prior to the measurements however, the relationship between the pressure in the reservoir p_{res} (pressure sensor (15)) and the pressure measured by sensor (16) was determined as a function of Q_{N_2}.

the O_2^-/O_3^- ion signals could be varied by tuning the operating conditions of the discharge.

NO_2^- ions were produced by charge transfer of SF_6^- to NO_2, which proceeds at a rate constant of 1.4×10^{-10} cm^3 molecule^{-1} s^{-1} [19]. The SF_6^- ions were formed by electron attachment to SF_6 introduced in the afterglow of an Ar discharge (3×10^{-3} STP cm^3 s^{-1} of a 5% mixture of SF_6, 3.3 STP cm^3 s^{-1} Ar). Sufficient amounts of NO_2 (1000 ppm mixture) were added to the buffer gas upstream the discharge, so that the charge exchange reaction was completed in the region upstream the reactant gas inlet.

Finally, O^- ions were generated by dissociative electron attachment of N_2O added to the afterglow of the Ar discharge (2×10^{-3} STP cm^3 s^{-1} of a 1000 ppm mixture of N_2O, 5 STP cm^3 s^{-1} Ar).

At room temperature, MSA has a very low vapor pressure ($p_{MSA} = 7.5 \times 10^{-4}$ mb at 298 K). In order to vary the concentration of MSA introduced into the flow tube over a range suitable for the study of ion/molecule reactions, it was necessary to heat the acid in a controlled way. MSA (purity 99.5+%, purchased from Sigma-Aldrich) was stored in a small glass reservoir, which was completely submerged in a water bath heated at 333.2 ± 0.1 K, to insure temperature uniformity. A flow of N_2 (purity 99.999%), circulating through a spiral shaped copper tube submerged in the heated water bath, passes through the glass reservoir, where it is saturated with MSA. The saturated flow is introduced into the flow tube by means of a finger inlet, located at 41 cm upstream of the mass spectrometer inlet (see Fig. 1). The short inlet line between the glass reservoir and the flow tube is kept at

a temperature slightly superior to the water bath temperature by heating tapes to prevent condensation of MSA in this inlet line. The much more abundant buffer gas in the flow tube quickly cools down the injected reactant gas to ambient temperature. The partial pressure of MSA in the flow tube was sufficient low, so that condensation should not occur. The flow of MSA, Q_{MSA}, introduced in the flow tube is given by:

$$Q_{MSA} = \frac{Q_{res}}{p_{res}} p_{MSA} \approx \frac{Q_{N_2}}{p_{res}} p_{MSA}, \quad Q_{N_2} \gg Q_{MSA}, \qquad (1)$$

where p_{MSA} is the vapor pressure of MSA in the reservoir at the temperature of the heated water bath. Q_{res} is the total flow through the reservoir, p_{res} is the total pressure in the reservoir and Q_{N_2} is the flow of nitrogen measured by a conventional flow meter. Q_{N_2} varied over a range from 5×10^{-3} to 0.18 STP cm^3 s^{-1}.

For the vapor pressure of MSA p_{MSA} to be used in Eq. (1) only few data are available in the literature. Clegg and Brimblecombe [20] reported a vapor pressure of $(1.00 \pm 0.27) \times 10^{-3}$ mb at 298 K. More recently, Tang and Munkelwitz [21] published measurements of MSA droplet evaporation rates in the temperature range from 299 up to 325 K. From these measurements they deduced the following values for the parameters A and B in the Clapeyron equation:

$$\ln(p_{MSA}) = A + \frac{B}{T}, \quad A = 23.10437, \; B = -9.03018 \times 10^3 \text{ K}, \qquad (2)$$

where T is the temperature in K and p_{MSA} is expressed in mb. It should be clear that the determination of p_{MSA} in our measurements relies heavily on above-mentioned values. No error estimations of A and B are reported by Tang and Munkelwitz [21].

Finally, the reaction time of the ions in the flow tube is measured by interrupting the ion flow with a voltage pulse on an electrically insulated grid in the vicinity of the reactant gas inlet and simultaneously recording the arrival of the disturbance of the ion swarm on the ion detector.

3. Results and discussion

3.1. Product ions

During the measurements involving O_2^- and O_3^- ions, the O_2^-/O_3^- ratio could be varied from 0 up to 7 by changing the operating conditions of the ion source. Both ions react with MSA by proton transfer:

$$O_2^- + CH_3SO_3H \rightarrow CH_3SO_3^- + \text{neutrals}, \qquad (3)$$

$$O_3^- + CH_3SO_3H \rightarrow CH_3SO_3^- + \text{neutrals}. \qquad (4)$$

In the cases where O_2^- was the most abundant source ion, small amounts of $O_2^- \cdot H_2O$ were present in the ion source mass spectra (±8% of the O_2^- signal). Reaction of $O_2^- \cdot H_2O$ with MSA also results in the formation of the $CH_3SO_3^-$ anion (95 u):

$$O_2^- \cdot H_2O + CH_3SO_3H \rightarrow CH_3SO_3^- + \text{neutrals}. \qquad (5)$$

Upon further addition of MSA, the $CH_3SO_3^-$ ion signal decreases and the secondary product ions $CH_3SO_3^- \cdot CH_3SO_3H$ (191 u) and $CH_3SO_3^- \cdot (CH_3SO_3H)_2$ (287 u) are formed, according to the following three body association reactions:

$$CH_3SO_3^- + CH_3SO_3H + M \rightarrow CH_3SO_3^- \cdot CH_3SO_3H + M, \qquad (6)$$

$$CH_3SO_3^- \cdot CH_3SO_3H + CH_3SO_3H + M \rightarrow CH_3SO_3^- \cdot (CH_3SO_3H)_2 + M. \qquad (7)$$

When studying the reaction of NO_3^- and $NO_3^- \cdot HNO_3$ with MSA, $CH_3SO_3^-$ and $CH_3SO_3^- \cdot HNO_3$ (158 u) were identified as primary product ions. Variation of the ratio $NO_3^-/NO_3^- \cdot HNO_3$ (from 1.3 up to 7) clearly showed that $CH_3SO_3^-$ is the product of the NO_3^-/MSA reaction, while the reaction of $NO_3^- \cdot HNO_3$ with MSA results in the formation of the $CH_3SO_3^- \cdot HNO_3$ product ion:

$$NO_3^- + CH_3SO_3H \rightarrow CH_3SO_3^- + \text{neutrals}, \qquad (8)$$

$$NO_3^- \cdot HNO_3 + CH_3SO_3H \rightarrow CH_3SO_3^- \cdot HNO_3 + \text{neutrals}. \qquad (9)$$

This is consistent with previous findings [22–24] that $NO_3^- \cdot (HNO_3)_{n=0,1}$ only reacts with those acids, which are stronger than HNO_3 (gas phase acidity of MSA is 1318 kJ mol^{-1} [25], whereas the gas phase acidity of HNO_3 = 1330 kJ mol^{-1} [26]).

At higher MSA concentrations, the $CH_3SO_3^- \cdot HNO_3$ ion signal decreases and the cluster ion $CH_3SO_3^- \cdot HNO_3 \cdot CH_3SO_3H$ (254 u) is observed:

$$CH_3SO_3^- \cdot HNO_3 + CH_3SO_3H + M \rightarrow CH_3SO_3^- \cdot HNO_3 \cdot CH_3SO_3H + M. \quad (10)$$

From our measurements, however, it is not clear whether the ligand switching reaction:

$$CH_3SO_3^- \cdot HNO_3 + CH_3SO_3H \rightarrow CH_3SO_3^- \cdot CH_3SO_3H + HNO_3, \quad (11)$$

can be excluded.

The evolution of the source and product ions vs. the MSA concentration for the reaction of NO_3^- and $NO_3^- \cdot HNO_3$ with MSA is shown in Fig. 2.

The reaction of NO_2^- with MSA proceeds by a proton transfer and an association channel:

$$NO_2^- + CH_3SO_3H \rightarrow CH_3SO_3^- + \text{neutrals}, \quad (12a)$$

$$NO_2^- + CH_3SO_3H + M \rightarrow NO_2^- \cdot CH_3SO_3H + M. \quad (12b)$$

From the ratio $NO_2^- \cdot CH_3SO_3H / CH_3SO_3^-$ obtained at 1.07 mb, a product ion distribution of 93 and 7% was found for reactions (12a) and (12b), respectively. Yields were determined at very low concentrations of the neutral reactant to minimize effects of secondary reactions and mass discrimination has been taken into account.

Upon further addition of MSA, the $NO_2^- \cdot CH_3SO_3H$ (142 u) ion signal decreases. Since $CH_3SO_3^- \cdot (CH_3SO_3H)_{n=1,2}$ are the only observed secondary reaction products, this decrease can be attributed to:

$$NO_2^- \cdot CH_3SO_3H + CH_3SO_3H \rightarrow CH_3SO_3^- \cdot CH_3SO_3H + \text{neutrals}. \quad (13)$$

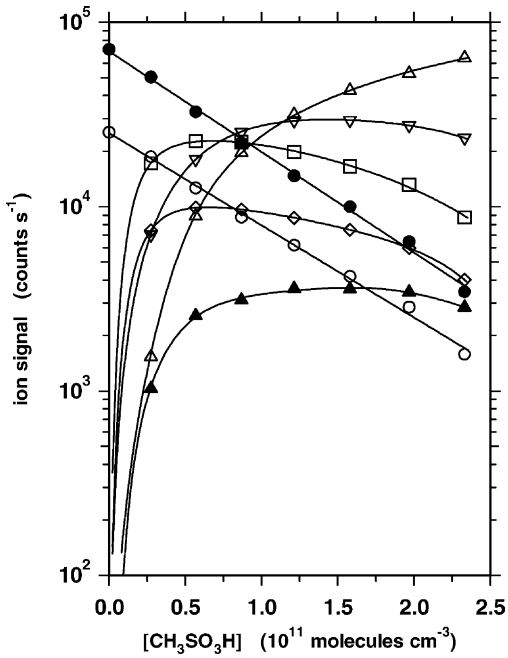

Fig. 2. Evolution of the count rate of the source and the product ions vs. the concentration of MSA in the flow tube for the reaction of NO_3^- and $NO_3^- \cdot HNO_3$ with MSA. (●) NO_3^-; (○) $NO_3^- \cdot HNO_3$; (□) $CH_3SO_3^-$; (▽) $CH_3SO_3^- \cdot CH_3SO_3H$; (△) $CH_3SO_3^- \cdot (CH_3SO_3H)_2$; (◇) $CH_3SO_3^- \cdot HNO_3$; (▲) $CH_3SO_3^- \cdot HNO_3 \cdot CH_3SO_3H$.

For the reaction of O^- with MSA, two pathways are observed: a proton transfer channel and a channel with additional subtraction of an H-atom:

$$O^- + CH_3SO_3H \rightarrow CH_3SO_3^- + \text{neutrals}, \quad (14a)$$

$$O^- + CH_3SO_3H \rightarrow CH_2SO_3^- + \text{neutrals}. \quad (14b)$$

Both pathways are almost equivalent: a 56–44% branching ratio was deduced.

Similar to $CH_3SO_3^-$ (reactions (6) and (7)), $CH_2SO_3^-$ (94 u) reacts with MSA to form the secondary cluster ions $CH_2SO_3^- \cdot CH_3SO_3H$ (190 u) and $CH_2SO_3^- \cdot (CH_3SO_3H)_2$ (286 u):

$$CH_2SO_3^- + CH_3SO_3H + M \rightarrow CH_2SO_3^- \cdot CH_3SO_3H + M, \quad (15)$$

$$CH_2SO_3^- \cdot CH_3SO_3H + CH_3SO_3H + M \rightarrow CH_2SO_3^- \cdot (CH_3SO_3H)_2 + M. \quad (16)$$

During the experiments with CO_3^- and CO_4^- source ions, the CO_4^-/CO_3^- ratio could be varied from 0 to 12. The reaction of CO_3^- with MSA gave rise to three product ions with $m/z = 95$, 126 and 156, which can be attributed to $CH_3SO_3^-$, $(CH_2SO_5)^-$ and $CO_3^-{\cdot}CH_3SO_3H$. As a rather high flow of molecular oxygen through the ion source was used for the production of the CO_3^- source ions, the O_2 concentration in the flow tube was quite high ($\sim 1 \times 10^{15}$ cm^{-3}) and the observed signal at $m/z = 126$ could correspond with ions resulting from the association of O_2 with $CH_2SO_3^-$. In this case $CH_2SO_3^-$ should be regarded as primary product, instead of $(CH_2SO_5)^-$. To verify this assumption, $CH_2SO_3^-$ ions were produced by the ion/molecule reaction of O^- with MSA, described in the preceding paragraph. Upon addition of O_2 (in the same concentration as during the experiments with CO_3^-) next to MSA, O^- also reacts with O_2 to form O_3^-. In the assumption that $CH_2SO_3^-$ does not cluster with O_2, the observed $CH_2SO_3^-$ signal will therefore be less than in the case where only MSA is introduced in the flow tube. Simple model calculations, assuming that $CH_2SO_3^-$ does not cluster with O_2, showed that under our experimental conditions the $CH_2SO_3^-$ signal drops by a factor 2 to 3 due to the reaction of O^- with O_2. Experimentally, however, upon addition of O_2 the $CH_2SO_3^-$ signal completely disappeared and ions with $m/z = 126$ were observed, which proves the association process of $CH_2SO_3^-$ with O_2. The CO_3^-/MSA reaction can therefore be summarized as follows:

$$CO_3^- + CH_3SO_3H \rightarrow CH_3SO_3^- + \text{neutrals}, \quad (17a)$$

$$CO_3^- + CH_3SO_3H \rightarrow CH_2SO_3^- + \text{neutrals} \quad (CH_2SO_3^- \cdot O_2 \text{ in presence of } O_2), \quad (17b)$$

$$CO_3^- + CH_3SO_3H + M \rightarrow CO_3^- \cdot CH_3SO_3H + M. \quad (17c)$$

At 1.07 mb, a 35–58–7% branching ratio was found for reactions (17a), (17b) and (17c), respectively. Secondary reaction products with $m/z = 222$ and 252 were also observed. Their formation can be explained by the following association reactions:

$$CO_3^- \cdot CH_3SO_3H + CH_3SO_3H + M \rightarrow CO_3^- \cdot (CH_3SO_3H)_2 + M, \quad (18)$$

$$CH_2SO_3^- \cdot O_2 + CH_3SO_3H + M \rightarrow CH_2SO_3^- \cdot O_2 \cdot CH_3SO_3H + M. \quad (19)$$

Our measurements, however, do not exclude the formation of $CH_3SO_3^-{\cdot}CH_3SO_3H$ by the reaction of $CO_3^-{\cdot}CH_3SO_3H$ with MSA.

In the study of CO_4^- with MSA $CH_3SO_3^-$ and $O_2^-{\cdot}CH_3SO_3H$ (128 u) were found to be the primary product ions with a 85–15% branching ratio:

$$CO_4^- + CH_3SO_3H \rightarrow CH_3SO_3^- + \text{neutrals}, \quad (20a)$$

$$CO_4^- + CH_3SO_3H \rightarrow O_2^- \cdot CH_3SO_3H + \text{neutrals}. \quad (20b)$$

Upon further addition of MSA the $O_2^-{\cdot}CH_3SO_3H$ ion signal decreases, probably through the reaction:

$$O_2^- \cdot CH_3SO_3H + CH_3SO_3H \rightarrow CH_3SO_3^- \cdot CH_3SO_3H + \text{neutrals}. \quad (21)$$

Table 1 gives an overview of the product ions and branching ratios of the different ion/molecule reactions studied. If thermodynamic data are available, the probable neutral products and the enthalpy change of the corresponding reaction $\Delta_r H^0$ are also listed. For the determination of the latter we rely upon the standard enthalpy of formation of the reactants and products as reported in [27] and the (-670 ± 10 kJ mol^{-1}) standard enthalpy of formation of MSA in the gas phase given by Guthrie et al. [28].

3.2. Rate constants

Rate constants have been derived from the source ion signal as a function of the MSA concentration and from the measured reaction time of the ions in the flow tube. The measured rate constants for the different ion/molecule reactions are listed in Table 2. Although we can take into account the errors on the measured

Table 1
Overview of the product ions and of the corresponding branching ratios for the different ion/molecule reactions

Ion/molecule reaction	Product ion	Neutral product(s)	Yield (%)	$\Delta_r H^0$ (kJ mol^{-1})
O^- + MSA	$CH_3SO_3^-$	OH	56	−149
	$CH_2SO_3^-$	–	44	–
O_2^- + MSA	$CH_3SO_3^-$	HO_2	100	−35
NO_2^- + MSA	$CH_3SO_3^-$	HNO_2	93	−166 ↔ +30
NO_2^- + MSA + M	$NO_2^-\cdot CH_3SO_3H$	–	7	–
O_3^- + MSA	$CH_3SO_3^-$	OH, O_2	100	+20 ↔ +58
$O_2^-\cdot H_2O$ + MSA	$CH_3SO_3^-$	H_2O, HO_2	100	+42
CO_3^- + MSA	$CH_3SO_3^-$	OH, CO_2	35	+20 ↔ +85
	$CH_2SO_3^-$	–	58	–
CO_3^- + MSA + M	$CO_3^-\cdot CH_3SO_3H$	–	7	–
NO_3^- + MSA	$CH_3SO_3^-$	HNO_3	100	−204 ↔ +92
CO_4^- + MSA	$CH_3SO_3^-$	HO_2, CO_2	85	+40 ↔ +72
	$O_2^-\cdot CH_3SO_3H$	–	15	–
$NO_3^-\cdot HNO_3$ + MSA	$CH_3SO_3^-\cdot HNO_3$	–	100	–

Probable neutral products are also listed, if thermodynamic data are available. However, several combinations of neutral products are possible for a given ion/molecule reaction. Since no literature data of the entropy change of the corresponding reactions are available, only those neutral products resulting in an exothermic reaction are listed. If all combinations result in endothermic reactions, the neutral products corresponding with the least endothermic reaction are given.

flows, pressures and on the experimentally determined reaction time, an estimation of the total accuracy of these rate constants is difficult, due to the fact that Tang and Munkelwitz [21] do not mention the errors on the parameters A and B, figuring in the Clapeyron Eq. (2) for MSA. If an error of 10% is assumed for p_{MSA}, the total accuracy (2 × S.D.) is estimated to be 30%. The precision of the measured rate constants is 10%.

Table 2
Rate constants for the ion/molecule reactions with MSA: k_{exp} are the experimentally determined values and k_{SC} are the collision rate constants obtained with the parameterized equation of Su and Chesnavich, based upon trajectory calculations (k, 10^{-9} cm^3 molecule^{-1} s^{-1})

Ion	k_{exp}	k_{SC}
O^-	4.1	5.3
O_2^-	3.4	4.0
NO_2^-	3.2	3.5
O_3^-	3.2	3.5
$O_2^-\cdot H_2O$	3.2	3.4
CO_3^-	2.9	3.2
NO_3^-	3.0	3.2
CO_4^-	3.0	3.0
$NO_3^-\cdot HNO_3$	2.7	2.7

Also listed in Table 2 are the collision rate constants k_{SC} calculated with the method of Su and Chesnavich [15], based upon trajectory calculations:

$$k_{SC} = k_L C(\alpha, \mu_D, T), \tag{22}$$

where k_L is given by the Langevin formula:

$$k_L = 2\pi q \sqrt{\frac{\alpha}{\mu}}, \tag{23}$$

with q the absolute value of the charge of the ion and μ the reduced mass of the ion/molecule system (all variables in atomic units). C is a parameterized equation, depending upon α, μ_D and T.

To our knowledge, no experimental data are available for the electric dipole moment μ_D and the polarizability α of MSA. In order to have an estimate of these parameters for the evaluation of k_{SC}, calculations were performed at the DFT/B3LYP level of theory (density functional theory using Becke's three-parameter nonlocal exchange functional [29] with the nonlocal

Table 3
Values of polarizability and dipole moment as obtained with different basis sets

Basis set	Dipole moment, μ_D (D)	Polarizability, α (Å^3)
cc-pVDZ	3.270	5.46
aug-cc-pVDZ	3.784	7.03
aug-cc-PVTZ	3.782	6.78
aug-cc-pVQZ	3.776	6.71

correlation functional of Lee et al. [30]). It is well known that the B3LYP method results in reliable values for the dipole moment [31]. Geometry optimizations of MSA were performed using several correlation consistent basis sets (cc-pVDZ, aug-cc-pVDZ, aug-cc-pVTZ, aug-cc-pVQZ [32–35]) and these were followed by the calculation of the Hessian to ensure that the obtained structure corresponds to a minimum.

As can be noticed in Table 3, the calculated values of μ_D and α converge with inclusion of more polarization functions and diffuse functions into the basis set. A value of 3.776 D for μ_D and of 6.71 Å^3 for α were obtained with the most extended basis set used (aug-cc-pVQZ). As a second approach to the determination of the dipole moment we have performed MP2 calculations with optimized geometry. Those lead to a value of 3.783 D, which is in excellent agreement with the B3LYP result.

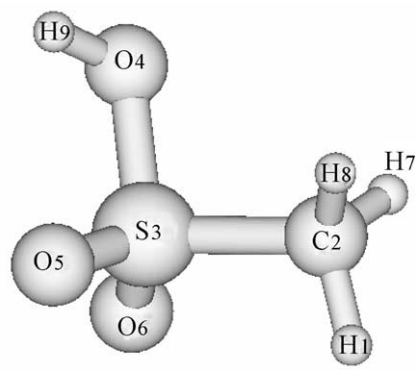

Fig. 3. Ground state geometry of methane sulfonic acid.

The equilibrium structure of MSA, optimized at the B3LYP/aug-cc-pVQZ level of theory, is shown in Fig. 3 and the obtained geometric parameters are shown in Table 4. All calculations were performed on a set of Linux PC's using the Gaussian 98 suite of programs [36].

Fig. 4 shows the measured rate constants together with the collision rate constants k_{SC}, calculated with the parameterized equation of Su and Chesnavich using a value of 3.776 D and 6.71 Å^3 for μ_D and α, respectively.

From this figure it is clear that the measured rate constants correspond within the experimental error with the calculated collision rate constants k_{SC}. In the

Table 4
Geometric parameters of methane sulfonic acid, calculated at the B3LYP/aug-cc-pVQZ level

Bond length		Bond angle		Dihedral angle	
H1–C2	1.0868	H1–C2–S3	106.5103	H1–C2–S3–O4	−176.9425
C2–S3	1.7821	H1–C2–H7	110.5627	H1–C2–S3–O5	70.3389
C2–H7	1.0858	H1–C2–H8	110.752	H1–C2–S3–O6	−64.4477
C2–H8	1.0855	S3–C2–H7	108.3955	H7–C2–S3–O4	−57.9536
S3–O4	1.6195	S3–C2–H8	108.9654	H7–C2–S3–O5	−170.6722
S3–O5	1.4411	H7–C2–H8	111.4867	H7–C2–S3–O6	54.5413
S3–O6	1.4324	C2–S3–O4	100.7786	H8–C2–S3–O4	63.5435
O4–H9	0.9668	C2–S3–O5	109.7369	H8–C2–S3–O5	−49.1751
		C2–S3–O6	108.6526	H8–C2–S3–O6	176.0384
		O4–S3–O5	107.0945	C2–S3–O4–H9	−113.4147
		O4–S3–O6	107.2353	O5–S3–O4–H9	1.3065
		O5–S3–O6	121.3488	O6–S3–O4–H9	133.011
		S3–O4–H9	107.9552		

Bond levels are given in Å and angles in degrees. Atom labels are given in Fig. 3.

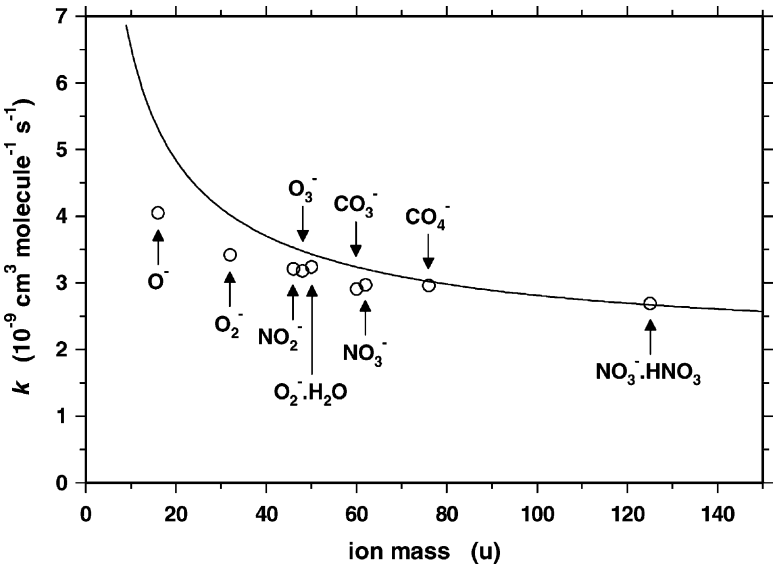

Fig. 4. Comparison between the experimentally determined rate constants k_{exp} (○) and the collision rate constants k_{SC}, calculated with the parameterized equation of Su and Chesnavich (solid line).

16–60 u mass range, however, the experimental values are systematically lower and the relative difference increases with decreasing mass (maximum 24% for O^-).

4. Conclusion

It is found that MSA reacts strongly with a variety of negative ions. Some of these reactions give multiple products, but all reactions studied are characterized by the formation of the $CH_3SO_3^-$ anion. The results of the kinetic study are summarized in Tables 1 and 2.

The ion/molecule reactions proceed within the experimental error at the collision rate. The measurements indicate, however, a systematic deviation from the collision rate constant towards slightly lower values for the reactions of MSA with ions in the mass range up to 60 u.

Eisele and Tanner [10], Weber et al. [11] and Mauldin et al. [12] report measurements of the concentration of MSA in the troposphere with the SICIMS technique (selected ion chemical ionization mass spectrometry). Since no literature data are available, they assume that the $NO_3^-{\cdot}HNO_3$/MSA reaction occurs at the same rate (collision rate) as the $NO_3^-{\cdot}HNO_3/H_2SO_4$ reaction, i.e., 2.3×10^{-9} cm^3 molecule^{-1} s^{-1} [13]. The latter only differs 15% from the value determined in this work. This implies that the reported tropospheric MSA concentrations are overestimated by only 15%, which is well within their experimental error.

Our measurements justify the use of $NO_3^- \cdot (HNO_3)_{n=0,1}$ as SICIMS source ion for the detection of MSA by chemical ionization mass spectrometry. CO_3^- and CO_4^- are also valid candidates, however the pressure dependence of the association channel (17c) has to be studied in detail.

In their model of the tropospheric ion composition Beig and Brasseur [14] incorporated, among many other ion/molecule reactions, the reaction of NO_3^- and $NO_3^-{\cdot}HNO_3$ with MSA, for which they assumed a rate constant of 2.5 and 2.0×10^{-9} cm^3 molecule^{-1} s^{-1}, respectively. As these values only differ by 17 and 26% from the experimentally determined rate constants, the use of the latter in the model will only result in minor changes.

References

[1] P.A. Spiro, D.J. Jacob, J.A. Logan, J. Geophys. Res. 97 (1992) 6023.
[2] T.S. Bates, B.K. Lamb, A. Guenther, J. Dignon, R.E. Stoiber, J. Atmos. Chem. 14 (1992) 315.
[3] S. Sharma, L.A. Barrie, D. Plummer, J.C. McConnell, P.C. Brickell, M. Levasseur, M. Gosselin, T.S. Bates, J. Geophys. Res. 104 (1999) 21327.
[4] S. Sørensen, H. Falbe-Hansen, M. Mangoni, J. Hjorth, N.R. Jensen, J. Atmos. Chem. 24 (1996) 299.
[5] C. Arsene, I. Barnes, K.H. Becker, R. Mocanu, Atmos. Environ. 35 (2001) 3769.
[6] M.O. Andreae, P.J. Crutzen, Science 276 (1997) 1052.
[7] S.M. Kreidenweis, J.H. Seinfeld, Atmos. Environ. 22 (1988) 283.
[8] R. Van Dingenen, F. Raes, J. Aerosol Sci. 24 (1993) 1.
[9] R.J. Charlson, J.E. Lovelock, M.O. Andreae, S.G. Warren, Nature 326 (1987) 655.
[10] F.L. Eisele, D.J. Tanner, J. Geophys. Res. 98 (1993) 9001.
[11] R.J. Weber, P.H. McMurry, F.L. Eisele, D.J. Tanner, J. Atmos. Sci. 52 (1995) 2242.
[12] R.L. Mauldin III, D.J. Tanner, J.A. Heath, B.J. Huebert, F.L. Eisele, J. Geophys. Res. 104 (1999) 5801.
[13] A.A. Viggiano, R.A. Perry, D.L. Albritton, E.E. Ferguson, F.C. Fehsenfeld, J. Geophys. Res. 87 (1982) 7340.
[14] G. Beig, G.P. Brasseur, J. Geophys. Res. 105 (2000) 22671.
[15] T. Su, W.J. Chesnavich, J. Chem. Phys. 76 (1982) 5183; T. Su, J. Chem. Phys. 89 (1988) 5355.
[16] D. Fussen, C. Amelynck, E. Arijs, Int. J. Mass Spectrom. Ion Processes 116 (1992) 13.
[17] C. Amelynck, D. Fussen, E. Arijs, Int. J. Mass Spectrom. Ion Processes 133 (1994) 13.
[18] O. Möhler, F. Arnold, J. Atmos. Chem. 13 (1991) 33.
[19] L.G. Huey, D.R. Hanson, C.J. Howard, J. Phys. Chem. 99 (1995) 5001.
[20] S.L. Clegg, P. Brimblecombe, Environ. Technol. Lett. 6 (1985) 269.
[21] I.N. Tang, H.R. Munkelwitz, J. Coll. Interf. Sci. 141 (1991) 109.
[22] F.L. Eisele, J. Geophys. Res. 94 (1989) 2183.
[23] D.J. Tanner, F.L. Eisele, J. Geophys. Res. 96 (1991) 1023.
[24] A.A. Viggiano, Mass Spectrom. Rev. 12 (1993) 115.
[25] I.A. Koppel, R.W. Taft, F. Anvia, S.-Z. Zhu, L.-Q. Hu, K.-S. Sung, D.D. DesMarteau, L.M. Yagupolskii, Y.L. Yagupolskii, N.V. Ignat'ev, N.V. Kondratenko, A.Y. Volkonskii, V.M. Vlasov, R. Notario, P.-C. Maria, J. Am. Chem. Soc. 116 (1994) 3047.
[26] S.G. Lias, J.E. Bartmess, J.F. Liebman, J.L. Holmes, R.D. Levin, G.W. Mallard, J. Phys. Chem. Ref. Data 17 (Suppl. 1) (1988) 1.
[27] NIST Chemistry WebBook, NIST Standard Reference Database Number 69, July 2001, P.J. Linstrom, W.G. Mallard (Eds.), National Institute of Standards and Technology, Gaithersburg, MD 20899 (http://webbook.nist.gov).
[28] J.P. Guthrie, A.R. Stein, A.P. Huntington, Can. J. Chem. 76 (1998) 929.
[29] A.D. Becke, J. Chem. Phys. 98 (1993) 5648.
[30] C. Lee, W. Yang, R.G. Parr, Phys. Rev. B37 (1988) 785.
[31] W. Koch, M.C. Holthausen, A Chemist's Guide to Density Functional Theory, 2nd ed., Wiley, New York, 2001.
[32] T.H. Dunning Jr., J. Chem. Phys. 90 (1989) 1007.
[33] R.A. Kendall, T.H. Dunning Jr., R.J. Harrison, J. Chem. Phys. 96 (1992) 6796.
[34] D.E. Woon, T.H. Dunning Jr., J. Chem. Phys. 98 (1993) 1358.
[35] D.E. Woon, T.H. Dunning Jr., J. Chem. Phys. 100 (1994) 2975.
[36] M.J. Frisch, G.W. Trucks, H.B. Schlegel, G.E. Scuseria, M.A Robb, J.R. Cheeseman, V.G. Zakrzewski, J.A. Montgomery Jr., R.E. Stratmann, J.C. Burant, S. Dapprich, J.M. Millam, A.D. Daniels, K.N. Kudin, M.C. Strain, O. Farkas, J. Tomasi, V. Barone, M. Cossi, R. Cammi, B. Mennucci, C. Pomelli, C. Adamo, S. Clifford, J. Ochterski, G.A. Petersson, P.Y. Ayala, Q. Cui, K. Morokuma, D.K. Malick, A.D. Rabuck, K. Raghavachari, J.B. Foresman, J. Cioslowski, J.V. Ortiz, A.G. Baboul, B.B. Stefanov, G. Liu, A. Liashenko, P. Piskorz, I. Komaromi, R. Gomperts, R.L. Martin, D.J. Fox, T. Keith, M.A. Al-Laham, C.Y. Peng, A. Nanayakkara, C. Gonzalez, M. Challacombe, P.M.W. Gill, B. Johnson, W. Chen, M.W. Wong, J.L. Andres, C. Gonzalez, M. Head-Gordon, E.S. Replogle, J.A. Pople, Gaussian 98, Revision A.7, Gaussian Inc., Pittsburgh, PA, 1998.